# Chapter 2
# Fractal Classification of Typical Meteorological Days from Global Solar Irradiance: Application to Five Sites of Different Climates

Samia Harrouni

## 1 Introduction

To electrify remote areas, the use of solar energy is the best economical and technological solution. The choice of the sites for the installation of photovoltaic systems and the analysis of their performances require the knowledge of the solar irradiation data. To meet these requirements, we have to classify the days into typical cases for a given site.

Many studies have investigated the problem of typical day's classification. These studies differ by the parameters used as criterion for the classification. This chapter presents a classification method of daily solar irradiances which is mainly based on fractals.

Fractals are objects presenting high degree of geometrical complexity, their description and modeling is carried out using a powerful index called fractal dimension. This later contains information about geometrical irregularities of fractal objects over multiple scales. The fractal dimension of a curve, for instance, will lie between 1 and 2, depending on how much area it fills. The fractal dimension can then be used to compare the complexity of two curves (Dubuc et al. 1989). In solar field, the fractal dimension is directly related to the temporal fluctuation of the irradiance signals. We can then quantify the solar irradiance fluctuations in order to establish a classification according to the atmospheric state (Maafi and Harrouni 2000, 2003; Harrouni and Guessoum 2003; Harrouni and Maafi 2002).

Our classification method defines two thresholds of the fractal dimensions using first a heuristic method then a statistical one. This allows determining three classes of days: clear sky day, partially clouded sky day and clouded sky day.

Samia Harrouni
Solar Instrumentation & Modeling Group/LIWS - Faculty of Electronics and Computer, University of Science and Technology H. Boumediene, Algiers, Algeria,
e-mail: sharrouni@yahoo.fr

This chapter is devoted to the fractal classification of typical meteorological days from global solar irradiances. We start in Section 2 with generalities on the solar radiation especially the most commonly used models to estimate the amount of radiation falling on a tilted plane. Then, we deal in the Section 3 with the problem of the fractal dimension estimation giving a short survey of existing methods. In Section 4, we present a new method to evaluate the fractal dimension of discrete temporal signals or curves with an optimization technique: the "Rectangular covering method". To evaluate its accuracy, the proposed method is applied to fractal signals whose theoretical fractal dimensions are known: Weierstrass function (WF) and fractional Brownian motion (FBM). Section 5 focuses on the classification of irradiances into typical days. This section begins with a survey of existing methods, and then the "Rectangular covering methods" is presented. Thereafter, we will be interested in the application of this method to five sites of different climates. Finally, in Section 6, we give a conclusion and discuss experimental results.

## 2 Solar Radiation

This section reviews the properties of solar radiation on Earth and summaries well-known models which are used to estimate the amount of radiation falling on a tilted plane.

Extraterrestrial solar radiation falling on a surface normal to the sun's rays at the mean sun earth distance is given by *solar constant* ($I_{sc}$). The current accepted value of $I_{sc}$ is 1367 $\mathrm{W/m^2}$.

When solar radiation enters the Earth's atmosphere, a part of the incident energy is removed by scattering or absorption by air molecules, clouds and particulate matter usually referred to as aerosols. The radiation that is not reflected or scattered and reaches the surface straight forwardly from the solar disk is called direct or beam radiation. The scattered radiation which reaches the ground is called diffuse radiation. Some of the radiation may reach a panel after reflection from the ground, and is called the ground reflected irradiation. In the Liu and Jordon approach the diffuse and ground reflected radiations are assumed to be isotropic. The total radiation consisting of these three components is called global or total radiation as shown in Fig. 2.1.

In many cases it is necessary to know the amount of energy incident on tilted surface, as shown in Fig. 2.1. However, measured total and diffuse radiation on horizontal surface are given in most available solar radiation databases. There are many models to estimate the average global radiation on tilted surfaces.

In this section we present the isotropic model developed by Liu and Jordan (Liu and Jordan 1963) which also estimates the average hourly radiation from the average daily radiation on a tilted surface.

The daily total radiation incident on a tilted surface $H_T$ can be written as

$$H_T = H_{b,T} + H_{d,T} + H_{r,T} \tag{2.1}$$

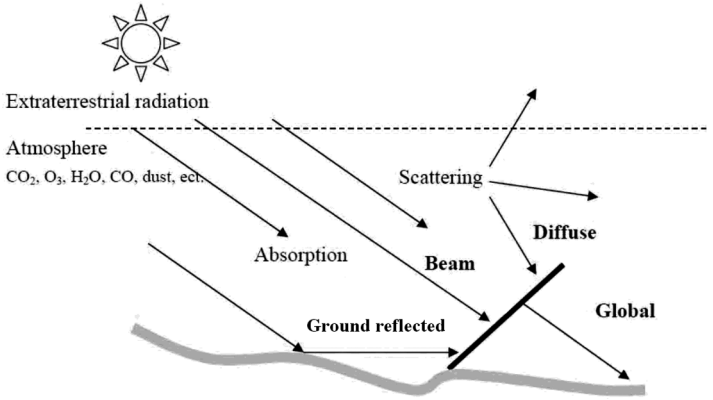


**Fig. 2.1** Solar radiation components

where $H_T$, $H_{b,T}$, $H_{d,T}$ and $H_{r,T}$ are daily total, beam, diffuse and ground reflected radiation, respectively, on the tilted surface.

In this model, (Liu and Jordan 1963) assumed that the intensity of diffuse radiation is uniform over the sky dome. Also, the reflected radiation is diffuse and assumed to be isotropic. Consequently, the daily total radiation on a tilted surface is given by

$$H_T = H_b R_b + H_d \left( \frac{1+\cos\beta}{2} \right) + H\rho \left( \frac{1-\cos\beta}{2} \right) \tag{2.2}$$

where $H_b$, $H_d$ and $H$ are daily beam, diffuse, total radiation, respectively, on a horizontal surface. $\beta$ represents a tilt angle, $\rho$ the ground albedo and $R_b$ the ratio of the daily beam radiation incident on an inclined plane to that on horizontal plane. For the northern hemisphere and south facing surfaces $R_b$ is given by

$$R_b = \frac{\cos(\phi-\beta)\cos\delta\sin\omega_s' + \omega_s'\sin(\phi-\beta)\sin\delta}{\cos\phi\cos\delta\sin\omega_s' + \omega_s\sin\phi\sin\delta} \tag{2.3}$$

where $\varphi$, $\delta$ and $\omega_s$ are the latitude, the declination and the sunset hour angle for the horizontal surface, respectively. $\omega_s$ is given by

$$\omega_s = \cos^{-1}(-\tan\phi\tan\delta) \tag{2.4}$$

$\omega_s'$ is the sunset hour angle for the tilted surface; it is given by

$$\omega_s' = \min\left\{\cos^{-1}(-\tan\phi\tan\delta), \cos^{-1}(-\tan(\phi-\beta)\tan\delta)\right\} \tag{2.5}$$

In the relation (2.3) $\omega_s$ and $\omega_s'$ are given in radian.

The daily clearness index $K_T$ is defined as the ratio of the daily global radiation on a horizontal surface to the daily extraterrestrial radiation on a horizontal surface. Therefore,

$$K_T = \frac{H}{H_0} \tag{2.6}$$

where $H_0$ is the daily extraterrestrial radiation on a horizontal surface. $H_0$ is given by (Sayigh 1977; Kolhe et al. 2003)

$$H_0 = \frac{24}{\pi} H_{sc} \left[ 1 + 0.033 \cos \left( \frac{2\pi j_d}{365} \right) \right] (\cos\phi \cos\delta \sin\omega_s + \omega_s \sin\phi \sin\delta) \quad (2.7)$$

where $j_d$ is the Julian day of the year.

Outside the atmosphere there is neither diffuse radiation nor ground albedo. $H_0$ is then assumed to be composed only of the beam radiation. Similarly, for tilted surfaces, the daily extraterrestrial radiation above the location of interest $H_{T0}$ is constituted only of direct component. Then, according to the relation

$$H_{bT} = H_b R_b \quad (2.8)$$

$H_{T0}$ can be computed as follows

$$H_{T0} = H_0 R_b \quad (2.9)$$

## 3 Fractal Dimension Estimation

### *3.1 Preliminaries*

Mathematically, any metric space has a characteristic number associated with it called *dimension*, the most frequently used is the so-called *topological* or *Euclidean* dimension. The usual geometrical figures have integer Euclidean dimensions. Thus, points, segments, surfaces and volumes have dimensions 0, 1, 2 and 3, respectively.

But what for the fractals objects, it is more complicated. For an example, the coastline is an extremely irregular line in such way that it would seem to have a surface, it is thus not really a line with a dimension 1, nor completely a surface with dimension 2 but, an object whose dimension is between 1 and 2. In the same way, we can meet fractals whose dimension ranges between 0 and 1 (Like the Cantor set which will be seen later) and between 2 and 3 (surface which tends to fill out a volume), etc. So, fractals have dimensions which are not integer but fractional numbers, called *fractal dimension*.

In the classical geometry, an important characteristic of objects whose dimensions are integer is that any curve generated by these elements contours has finite length. Indeed, if we have to measure a straight line of 1 m long with a rule of 20 cm, the number of times that one can apply the rule to the line is 5. If a rule of 10 cm is used, the number of application of the rule will be 10 times, for a rule of 5 cm, the number will be 20 times and so on. If we multiply the rule length used by the number of its utilization we will find the value 1 m for any rule used.

This result if it is true for the traditional geometry objects, it is not valid for the fractals objects. Indeed, let us use the same way to measure a fractal curve,

with a rule of 20 cm, the measured length will be underestimated but with a rule of 10 cm, the result will be more exact. More the rule used is short more the measure will be precise. Thus, the length of a fractal curve depends on the rule used for the measurement: the smaller it is, the more large length is found.

It is the conclusion reached by Mandelbrot when he tried to measure the length of the coast of Britain (Mandelbrot 1967). He found that the measured length depends on the scale of measurement: the smaller the increment of measurement, the longer the measured length becomes.

Thus, fractal shapes cannot be measured with a single characteristic length, because of the repeated pattern we continuously discover at different scale levels.

This growth of the length follows a power law found empirically by Richardson and quoted by Benoît Mandelbrot in his 1967 paper (Richardson 1961)

$$L(\eta) \propto \eta^{-\alpha} \tag{2.10}$$

where $L$ is the length of the coast, $\eta$ is the length of the step used, the exponent $\alpha$ represents the fractal dimension of the coast.

Other main property of fractals is the self-similarity. This characteristic means that an object is composed of sub-units and sub-sub-units on multiple levels that resemble the structure of the whole object. So fractal shapes do not change even when observed under different scale, this nature is also called scale-invariance. Mathematically, this property should hold on all scales. However, in the real world the self-similarity is only observed over some scales the objects are then statistically self-similar or self-affine.

## 3.2 Experimental Determination of the Fractal Dimension of Natural Objects

Fractal dimension being a measurement in the way in which the fractal occupies space, to determine it we have to draw up the relationship between this way of occupation of space and its variation of scale. If a linear object of size $L$ is measured with a self-similar object of size $l$, then number of self similar objects within the original object $N(l)$ is related to $L/l$ as

$$N = \left(\frac{L}{l}\right)^{D} \tag{2.11}$$

where $D$ is the fractal dimension. From where

$$D = \frac{\ln(N)}{\ln\left(\frac{L}{l}\right)} \tag{2.12}$$

For the self-similar fractals, $L/l$ represents the magnification factor and $l/L$ the reduction factor. Nevertheless, when one tries to determine fractal dimension of

natural objects, one is often confronted with the fact that the direct application of Eq. (2.12) is ineffective. In fact, the majority of the natural fractal objects existing in our real world are not self-similar but rather self-affine. The magnification factor and the reduction factor are thus difficult to obtain since there is not an exact self-similarity. Other methods are then necessary to estimate the fractal dimensions of these objects.

In practice, to measure a fractal dimension, several methods exist, some of which are general, whereas others are applicable only to special classes of fractals. This section, focuses on the more commonly used methods namely, Box-counting dimension and Minkowski–Bouligand dimension which are based on the great works of Minkowski and Bouligand (Minkowski 1901; Bouligand 1928) and from which derive several other algorithms.

**Box–counting dimension:** This method is based upon a quantization of the space in which the object is imbedded by a grid of squares of side $\varepsilon$. The number $N(\varepsilon)$ of squares that intersect the fractal object is then counted. The Box-counting dimension is then defined by

$$D_B = \lim_{\varepsilon \to 0} \frac{\ln [N(\varepsilon)]}{\ln \left(\frac{1}{\varepsilon}\right)} \tag{2.13}$$

If one plots $\ln(N(\varepsilon))$ versus $\ln(1/\varepsilon)$, the slope of the straight line gives the estimate of the fractal dimension $D_B$ in the box-counting method.

Figure 2.2 gives an example illustrating this method. The object $E$ (a curve) is covered by a grid of squares of side $\varepsilon_1 = 1/20$, and for this value of $\varepsilon$ total number of squares contained in the grid is $20^2 = 400$ and the number of squares intersecting the curve $E$ is 84 (Fig. 2.2a). In Fig. 2.2b, which is obtained using different values of $\varepsilon$, the slope of the straight line fitted by a linear regression constitutes the fractal dimension of the curve $E$.

**Minkowski–Bouligand dimension:** This method is based on Minkowski's idea of dilating the object which one wants to calculate the fractal dimension with disks of radius $\varepsilon$ and centered at all points of $E$. The union of these disks thus creates a *Minkowski cover*.

Let $S(\varepsilon)$ be the surface of the object dilated or covered and $D_M$ the Minkowski–Bouligand dimension. Bouligand defined the dimension $D_M$ as follows

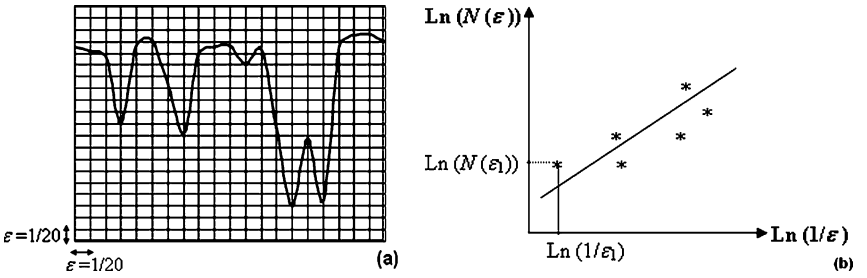


**Fig. 2.2** Example illustrating the Box -counting method **a)** Covering the curve by a grid of squares **b)** The log-log plots

$$D_M = 2 - \lambda\,(S) \tag{2.14}$$

where $\lambda(S)$ is the similarity factor and it represents the infinitesimal order of $S(\varepsilon)$. It is defined by

$$\lambda\,(S) = \lim_{\varepsilon \to 0} \frac{\ln\left[S\left(\varepsilon\right)\right]}{\ln\left(\varepsilon\right)} \tag{2.15}$$

Inserting Eq. (2.15) in Eq. (2.14) we obtain

$$D = \lim_{\varepsilon \to 0} \left[\frac{2 - \ln\left[S\left(\varepsilon\right)\right]}{\ln\left(\varepsilon\right)}\right] \tag{2.16}$$

The properties of the logarithm permit us to rewrite the relation (2.16) in the following form

$$D = \lim_{\varepsilon \to 0} \frac{\ln\left[\frac{S(\varepsilon)}{\varepsilon}\right]}{\ln\left(\frac{1}{\varepsilon}\right)} \tag{2.17}$$

or, rearranged

$$\ln\left(\frac{S\left(\varepsilon\right)}{\varepsilon}\right) = D \ln\left(\frac{1}{\varepsilon}\right) + \text{constant, as } \varepsilon \to 0 \tag{2.18}$$

The fractal dimension can then be estimated by the slope of the log–log plot: $\ln\left(S\left(\varepsilon\right)/\varepsilon\right) = f\left(\ln\left(1/\varepsilon\right)\right)$ fitted by the least squares method. Figure 2.3a shows the Minkowski covering $E(\varepsilon)$ composed of the union of disks of radius $\varepsilon$.

## 3.3 Discussion of the Two Methods

According to the analysis of Dubuc et al. (Dubuc et al. 1989), the Box–counting dimension and the Minkowski–Bouligand dimension are mathematically equivalent

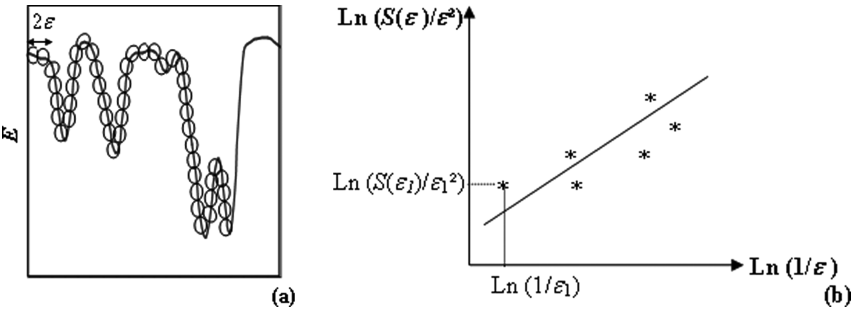


**Fig. 2.3** Example illustrating the Minkowski–Bouligand method **a)** The Minkowski covering **b)** The log–log plots

in limit thus, $D_B = D_M$. However, they are completely different in practice because of the way that limits are taken, and the manner in which they approach zero.

Experimental results published in the literature (Dubuc et al. 1989; Maragos and Sun 1993; Zeng et al. 2001) showed that these two methods suffer from inaccuracy and uncertainty. Indeed, according to Zeng et al. (2001) the precision of these estimators are mainly related to the following aspects:

- **Real Value of the Fractal Dimension *D*:** With big values of $D$, the estimation error is always very high. This can be explained by the effect of resolution (Huang et al. 1994). When the value of $D$ increases, its estimates can not reflect the roughness of the object and higher resolution is then needed.
- **Resolution:** In the case of the temporal curves, the resolution consists of observation size of the curve (minute, hour, day…). According to Tricot et al. (1988) estimated fractal dimension decreases with the step of observation. This is due to the fact that a curve tends to become a horizontal line segment and appears more regular.
- **Effect of Theoretical Approximations:** Imprecision of the Box-counting and the Minkowski-Bouligand methods is also related to constraints occurring in theoretical approximations of these estimators. For example, the Box-counting dimension causes jumps on the log-log plots (Dubuc et al. 1989) which generate dispersion of the points of the log-log plots with respect to the straight line obtained by linear regression. Moreover, the value of $N(\varepsilon)$ must be integer in this method. The inaccuracy of the method of Minkowski-Bouligand is due to the fact that the Minkowski covering is too thick.
- **Choice of the Interval $[\varepsilon_0, \varepsilon_{max}]$**: The precision of the estimators is influenced much by the choice of the interval $[\varepsilon_0, \varepsilon_{max}]$ through which the line of the log-log plots is adjusted. $\varepsilon_o$ is the minimum value that can be assigned to the step. When $\varepsilon_0$ is too large, the curve is covered per few elements (limp or balls). Conversely, when the value $\varepsilon_{max}$ is too small, the number of elements which cover the curve is too large and each element covers few points or pixels. Some researchers tried to choose this "optimal" interval in order to minimize the error in estimation (Dubuc et al. 1989; Huang et al. 1994). For example, Liebovitch and Toth (1989) proposed a method for determining this interval, Maragos and Sun (1993) used an empirical rule to determine $\varepsilon_{max}$ for temporal signals. In practice, these optimal intervals improve considerably the precision of the fractal dimension estimate for special cases but not in all cases.

# 4 Measuring the Fractal Dimension of Signals

## *4.1 A Survey of Existing Methods*

Many natural processes described by time series (e.g., noises, economical and demographic data, electric signals… etc.) are also fractals in the sense that their graph

is a fractal set (Maragos and Sun 1993). Thus, modeling fractal signals is of great interest in signal processing.

Considering the importance of this index and the impact of its use in practice, the precision of its estimate is necessary. Methods of Box–counting and of Minkowski–Bouligand prove then ineffective due to the fact that they suffer from inaccuracy as we already mentioned. Inspired by the Minkowski–Bouligand method, a class of approaches to compute the fractal dimension of signal curves or one-dimensional profiles called "covering methods" is then proposed by several researchers.

These methods consist in creating multiscale covers around the signal's graph. Indeed, each covering is formed by the union of specified structuring elements. In the method of Box–counting, the structuring element used is the square or limp, that of Minkowski–Bouligand uses the disk.

Dubuc et al. (1989 and Tricot et al. (1988) proposed a new method called "Variation method". This one criticizes the standard methods of fractal dimension estimation namely: Box–counting and Minkowski–Bouligand. Indeed, "Variation method" applied to various fractal curves showed a high degree of accuracy and robustness.

Maragos and Sun (1993) generalized the method of Minkowski–Bouligand by proposing the "Morphological covering method" which uses multiscale morphological operations with varying structuring elements. Thus, this method unifies and improves other covering methods. Experimentally, "Morphological covering method" demonstrated a good performance, since it has experimentally been found to yield average estimation errors of about 2%–4% or less for discrete fractal signals whose fractal dimension is theoretically known (Maragos and Sun 1993). For deterministic fractal signals (these signals will be detailed further in this chapter) Maragos and Sun developed an optimization method which showed an excellent performance, since the estimation error was found between 0 % and 0.07 %.

## *4.2 New Method for Estimating the Fractal Dimension of Discrete Temporal Signals*

In order to contribute in improving the accuracy of fractal dimension estimation of the discrete temporal signals we developed a simple method based on a covering by rectangles called Rectangular Covering Method.

### Presentation of the Method

The method based on Minkowski–Bouligand approach consists in covering the curve for which we want to estimate fractal dimension by rectangles. The choice of this type of structuring element is due to the discrete character of the studied signals.

From the mathematical point of view, the use of the rectangle as structuring element for the covering is justified. Indeed, Bouligand (1928) showed that $D_M$

(Minkowski–Bouligand dimension) can be obtained by also replacing the disks in the previous covers with any other arbitrarily shaped compact sets that posses a nonzero minimum and maximum distance from their center to their boundary.

Thus, as shown in Fig. 2.4, for different time intervals $\Delta\tau$, the area $S(\Delta\tau)$ of this covered curve is calculated by using the following relation

$$S(\Delta\tau) = \sum_{n=0}^{N-1} \Delta\tau \left| f(t_n + \Delta\tau) - f(t_n) \right| \tag{2.19}$$

where $N$ denotes the signal length, $f(t_n)$ is the value of the function representing the signal at the time $t_n$ and $|f(t_n + \Delta\tau) - f(t_n)|$ is the function variation related to the interval $\Delta\tau$. The fractal dimension is then deduced from Eq. (2.20) where $\varepsilon$ is replaced by the time interval $\Delta\tau$. Hence

$$\ln\left(\frac{S(\Delta\tau)}{\Delta\tau}\right) = D \ln\left(\frac{1}{\Delta\tau}\right) + \text{constant, as } \Delta\tau \to 0 \tag{2.20}$$

Thus, to determine the fractal dimension $D$ which represents the slope of the straight line of Eq. (2.20), it is necessary to use various time scales $\Delta\tau$ and to measure the corresponding area $S(\Delta\tau)$. We then obtain several points $(\Delta\tau_i, S(\Delta\tau_i))$ constituting the line.

A good estimation of the fractal dimension $D$ requires a good fitting of the log-log plot defined by Eq. (2.20). Therefore, the number of points constituting the plot is important. This number is fixed by $\Delta\tau_{max}$ which is the maximum interval through which the line of the log-log plots is fitted.

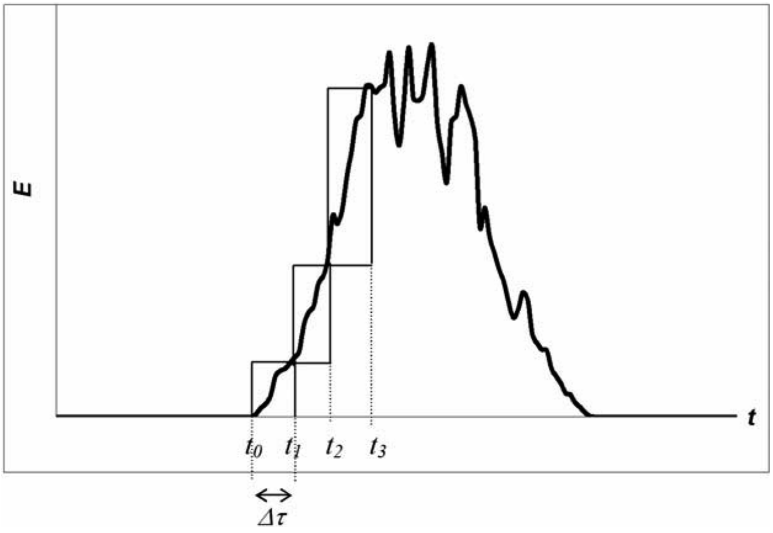


**Fig. 2.4** An example of temporal curve covered by rectangles

As mentioned above, to estimate the fractal dimension most of methods determine $\Delta\tau_{max}$ experimentally. This procedure requires much time and suffers from precision. Also, we developed an optimization technique to estimate $\Delta\tau_{max}$.

### Optimization Technique

Experience shows that $\Delta\tau_{max}$ required for a good estimation of $D$ depends on several parameters, especially the time length of the signal $N$. $\Delta\tau$ should not be too weak, in order not to skew the fitting of the line, and it must not exceed $N/2$. $\Delta\tau$ must also satisfy the condition of linearity of the line.

Our optimization technique (Harrouni et al. 2002) consists first in taking a $\Delta\tau_{max}$ initial about 10, because the number of points constituting the plot should not be very small as signaled above; then, $\Delta\tau_{max}$ is incremented by step of 1 until $N/2$. We hence obtain several straight log-log lines which are fitted using the least squares estimation. The $\Delta\tau_{max}$ optimal is the one corresponding to the log-log straight line with the minimum least square error. This later is defined by the following formula

$$E_{quad} = \frac{\sum_{i=1}^{n} d_i}{n} \tag{2.21}$$

In this relation $n$ denotes the number of points used for the straight log–log line fitting, $d_i$ represents the distance between the points $\left(\ln\left(1/\Delta\tau\right), \ln\left(S\left(\Delta\tau\right)/\Delta\tau^2\right)\right)$ and the fitted straight log–log line.

### Validation of the Method

In order to test the validity and the accuracy of the rectangular covering method, we applied it to two different types of parametric fractal signals whose theoretical fractal dimension is known, these test signals are the Weirstrass function (WF) which is a deterministic signal and the random signal of the fractional Brownian motion (FBM). These fractal signals that will be briefly defined below are most commonly used in various applications.

**The Weierstrass Function (FW):** It is defined as (Hardy 1916; Mandelbrot 1982; Berry and Lewis 1980)

$$W_H(t) = \sum_{k=0}^{\infty} y^{-kH} \cos\left(2\pi y^k t\right), \text{ as } 0 < H < 1 \tag{2.22}$$

This function is continuous but nowhere differentiable; $\gamma$ is an integer such as $\gamma > 1$. This parameter is fixed by the experimenter so that he can choose the shape of the signal, the fractal dimension of this function is $D = 2 - H$. In our experiments, we synthesized discrete time signals from WF's by sampling $t \in [0,1]$ at $N+1$ equidistant points, using $\gamma = 2.1$ and truncating the infinite series so that the summation is

done only for $0 \leq k \leq k_{max}$. The $k_{max}$ is determined by the inequality $2\pi\gamma k \leq 10^{12}$ established by Maragos and Sun (1993).

**Fractional Brownian Motion (FBM):** It is one of the most mathematical models used to describe self-affine fractals existing in nature. Mandelbrot and Wallis proposed an extension of this motion: the fractional Brownian motion. The function of the Brownian fractional motion $B_H(t)$ with parameter $0 < H < 1$ is a time varying random function with stationary, Gaussian distributed, and statically self-affine increments. So

$$\left\langle [B_H(t) - B_H(t_0)]^2 \right\rangle = 2D(t - t_0)^{2H}, \text{ as } 0 < H < 1 \tag{2.23}$$

The fractal dimension $D$ of $B_H(t)$ is $D = 2 - H$. To synthesize FBM signals, several methods exist (Mandelbrot and Wallis 1969; Voss 1988; Lundahl and all. 1986) the most known are: Choleski decomposition method, Durbin–Levinson algorithm, FFT method and circulant matrix method. In our experiments we synthesized FBM signals via the Durbin–Levinson method.

To validate our rectangular covering method we applied it to these synthesized test signals. For this purpose, the error between the theoretical fractal dimension and the estimated one is used. The experimental results indicate that, for the two fractal signals WF and FBM, the rectangular covering method performs well in estimating dimensions $D \in [1.1, 1.9]$, since the estimation error is less than or equal 6 % for the WF signals and 7 % for FBM signals (Harrouni and Guessoum 2006). By varying the signals' length $N \in [100, 1000]$ with a step of 100 we have also observed similar performance of this method. Over 99 different combinations of ($D$, $N$) the average estimation error of the rectangular covering method was 4 % for both WF's and FBM's.

## 5 Classification of the Solar Irradiances to Typical Days

### *5.1 A Survey of Existing Methods*

Modeling random fluctuations of the solar irradiance has already been the object of several studies published in the literature. These are based mostly on the random processes. The Markovian approaches in particular, contributed extensively to this modeling. One can see for example, the works of Brinkworth (1977), Bartoli et al. (1981), Lestienne et al. (1979), Aguiar et al. (1988) and Maafi (1991). This last reference treated the problem of the classification of the insolation and the daily irradiation indirectly by joining them to the states of the sky: clear sky, covered sky, etc. (Maafi 1991, 1998).

Other statistical methods were used for classification of typical meteorological days such as automatic classification (Bouroubi 1998), the analysis of the correlations (Louche and al. 1991) and the Ward's method (Muselli et al. 1991).

More recent studies are interested by the modeling of the random character of the solar radiation using neural networks (Guessoum et al. 1998; Sfetsos and Coonick 2000). In addition to the originality of these new approaches, these studies aim to value the contribution of their formalisms in the description of the solar radiation fluctuating character.

However, very few works treating the classification of the solar radiation signals using the fractal analysis were published (Maafi and Harrouni 2000, 2003; Harrouni and Guessoum 2003; Harrouni and Maafi 2002; Louche et al. 1991). In this section the contribution of the fractal analysis to the classification of the solar irradiance signals is given. This examination leads to the determination of different sky types in a given time interval as: clear sky, partially covered sky, covered sky etc. which is useful for planning and analyzing solar energy systems. Hence, a classification method is proposed which allows the categorization of the solar radiation fluctuations based on the fractal dimension (Harrouni et al. 2005).

## *5.2 Fractal Classification of Solar Irradiance*

### Methodology

Our method classification uses the fractal dimension as a basic criterion to achieve the classification of the solar irradiance and to yield different types of days, i.e., clear sky day, covered sky day, a cloudy day, etc. Our research reveals that some daily solar irradiance signals have the same fractal dimension but corresponding to days with different weather conditions. Indeed, a uniformly cloudy day and a sunny one have regular irradiance shapes and practically the same value for $D$ but have daily different clearness indexes. That is why the daily clearness index $K_T$ is calculated along with $D$ as a second criterion in the categorization algorithm which allows sorting daily irradiances into three classes according to the following classification:

Class I: Clear sky day
$1 \leq D \leq D_I$ and $K_T \geq (K_T)_I$
Class II: Partially cloudy sky
$D_I < D \leq D_{II}$ and $K_T \geq (K_T)_I$
Class III: Completely cloudy sky
$D > D_{II}$ or $D \leq D_{II}$ and $K_T < (K_T)_I$

$D_I$, $D_{II}$, are the thresholds for $D$ and $(K_T)_I$ is the one for $K_T$ for the different classes.

The thresholds for $D$ and $K_T$ are new parameters to be determined in order to achieve the classification of the irradiances. The value 0.5 is chosen for $(K_T)_I$; this value permits to distinguish the covered sky day class from the one of clear sky day. Indeed, experimental results reveals that for some days of class III (covered sky day), the fractal dimension $D$ is closer to 1, this is due to the fact that these days are so covered that the corresponding irradiance curve is regular but the clearness index is very low (lower than 0.5).

To determine the thresholds of the fractal dimension $D_I$ and $D_{II}$ we first used a heuristic approach then a statistical one. The heuristic approach consists in analyzing all daily solar irradiances shapes and their corresponding fractal dimension. For each day of the year the histograms of the irradiance signals are constructed. These histograms are built by class of $100\,\mathrm{W/m^2}$. By observing their various forms, i.e. preponderance of low or high frequencies, we noted that there were three kinds of histograms (Maafi and Harrouni 2003):

- Histograms in the shape of J
- Histograms in the shape of U
- Histograms in the shape of L

By identifying the relations of classification established above with these three types of histograms, we can determine the $D$ thresholds correspondent to the three classes. (An example of these histograms is given for Tahifet on the accompanying CD).

The statistical method is based on the cumulative distribution function (CDF) $F_X(x)$. This latter describes the probability distribution of a real-valued random variable $X$. For every real number $x$, the CDF of $X$ is the probability that the random variable $X$ takes on a value less than or equal to $x$. Thus, the two thresholds of $D$ correspond respectively to the fractal dimension whose the cumulative distribution function $F_X(x)$ are:

$$F_x(x) = \frac{\max(F_x(x)) - \min(F_x(x))}{3} \text{ and} \tag{2.24}$$

$$F_x(x) = \frac{2(\max(F_x(x)) - \min(F_x(x)))}{3}$$

## Data Bank

The experimental database contains global irradiance data measured at five sites of different climates. Two south Algerian sites: Tahifet (Tamanrasset) and Imehrou (Illizi), two sites of Colorado: Golden and Boulder and the last site is Palo Alto located in California.The geographical coordinates of these sites are given in Table 2.1.

Algerian sites data are recorded from the operation of two stand-alone photovoltaic power installations during 1992-year on a 10°-tilted surface with a time step of 10 minutes. These systems have been installed by the National Company from

**Table 2.1** Geographical coordinates of the studied sites

| Site | Latitude | Longitude | Altitude (m) |
|---|---|---|---|
| Tahifet | 22°53′N | 06°00′E | 1400 |
| Imehrou | 26°00′N | 08°50′E | 600 |
| Golden | 39°74′N | 105°18′W | 1829 |
| Boulder | 39°91′N | 105°25′W | 1855 |
| Palo alto | 37°42′N | 122°.15′W | 12.192 |

Electricity and Gaz (SONELGAZ). For Colorado sites the irradiance data have been collected during the year 2003 on a horizontal surface. These data are provided by MIDC (Measurement and Instrumentation Data Center) (MIDC, 2007). Data at Palo Alto have been recorded from the operation of one grid-connected system during 2003-year on a 30°-tilted surface with a time step of 15 minutes. This PV system was installed in May 2000 by CPAU (City of Palo Alto utilities) (CPAU, 2007).

By integrating the measured irradiances we determined the daily irradiation. Then, we calculated the daily clearness index $K_T$ using Eq. (2.6). The measured daily global and extraterrestrial irradiation together with daily clearness index for all studied sites are included on the accompanying CD.

$H_0$ is calculated by using Eq. (2.7) for irradiations received on horizontal surface (Boulder and Golden) and Eq. (2.9) for irradiations on tilted plane (Tahifet, Imehrou and Palo Alto).

## Fractal Treatment of Solar Irradiances

Figure 2.5 presents two examples of the log–log lines permitting the estimation of the fractal dimension of irradiance curves. This figure shows that the log–log points are grouped around the fitting line which demonstrates the self affinity of the studied solar irradiances.

The fractal dimensions obtained from the slopes of the log–log lines for all sites are given in the accompanying CD. Figure 2.6 gives representative examples for the daily irradiation values corresponding to different fractal dimensions from three classes. As can be observed there is good correspondences between the shapes of the signals and the corresponding fractal dimensions.

Figure 2.7 gives the annual evolution of the monthly average of $D$ for the studied sites. This figure shows clearly that $D$ fluctuates.

In order to quantify this fluctuation we calculated the annual average $<D>$ of the fractal dimension and the corresponding standard deviation $\sigma$ which are tabulated in Table 2.2. These values suggest that the solar irradiances of Tahifet and Boulder exhibit the similar fluctuations ($<D> = 1.16$ for Tahifet and 1.13 for Imehrou).

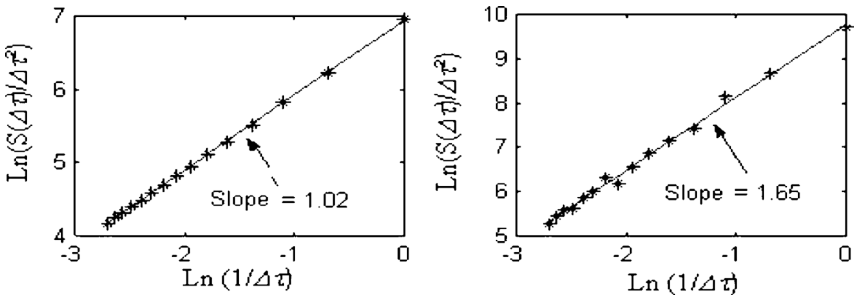


**Fig. 2.5** Two examples (Golden site) of log–log plots fitted by the least-squares estimation with their slopes which represent the estimated fractal dimension

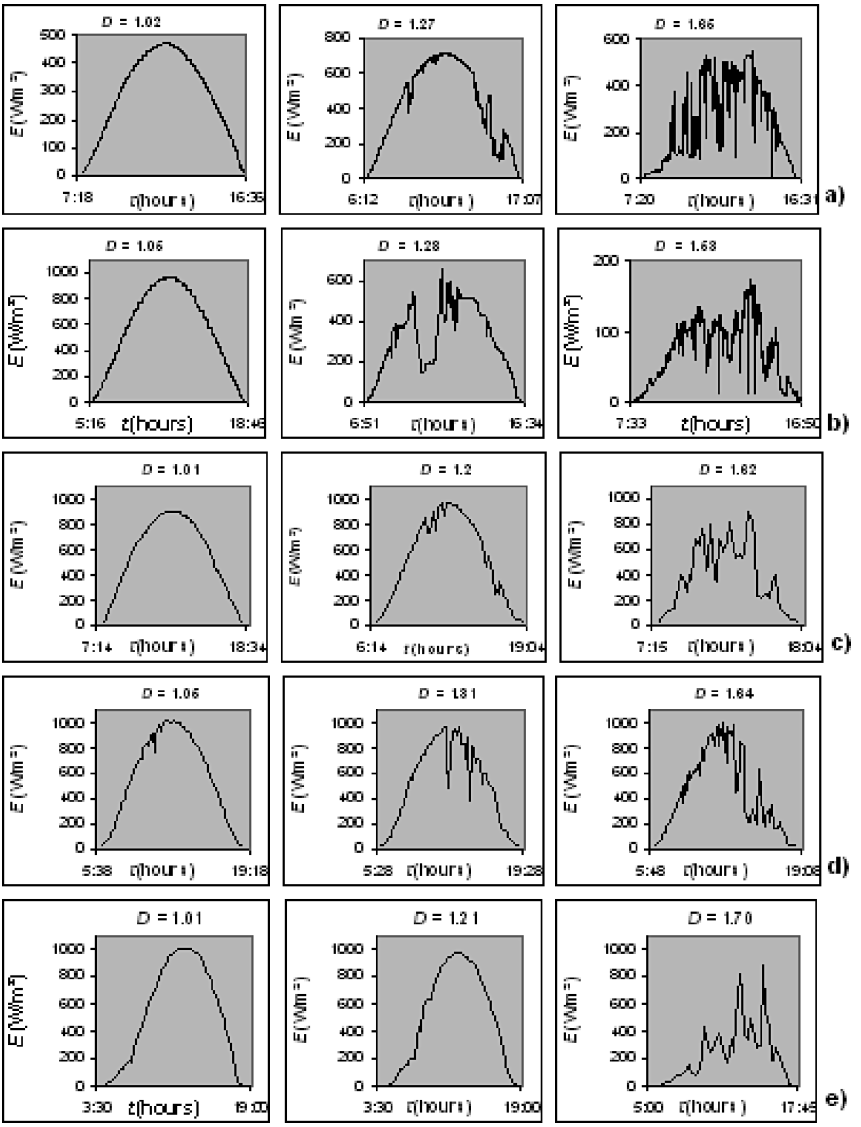


**Fig. 2.6** Typical daily irradiance values for the three classifications and fractal dimensions for the sites under consideration **a)** Golden, **b)** Boulder, **c)** Tahifet, **d)** Imehrou, **e)** Palo Alto

This is also observed for Golden and Boulder ($<D> = 1.38$ for Golden and 1.39 for Boulder). To compare the degree of fluctuation of the solar irradiances of the different sites we can refer to the values of $<D>$. Hence, the two sites of Colorado are fluctuating, those of the Algerian sites fluctuate slightly, they are practically regular, and in Palo Alto irradiances are fairly fluctuating. However, the analysis of $D$ month by month permits the detection of the months where the fluctuations of the irradiances are most intense – June and December for Tahifet, March and June for

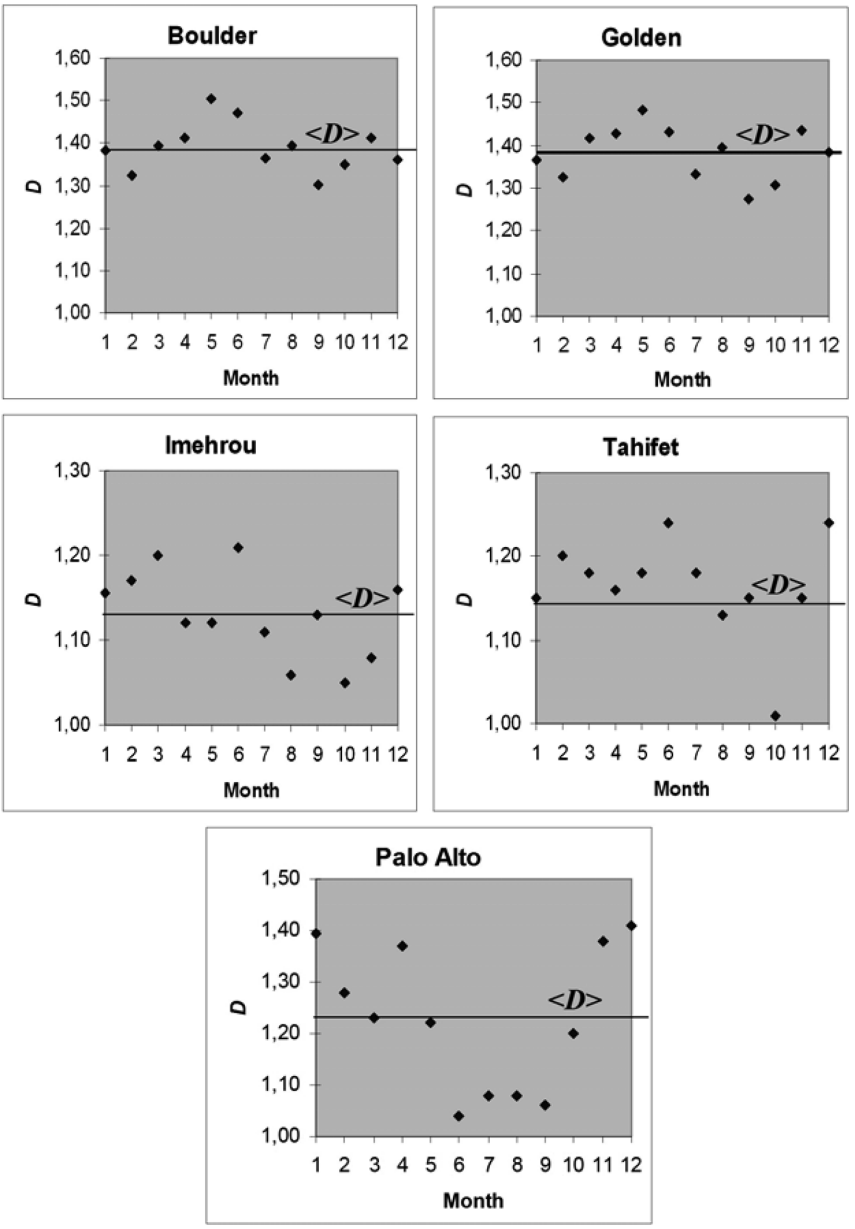


**Fig. 2.7** Annual variation of the monthly means of the estimated fractal dimension $D$, the straight solid line represents the annual mean of the fractal dimension $<D>$

**Table 2.2** Annual averages $<D>$ and standard deviations $\sigma$ of the estimated fractal dimensions

| Site | $<D>$ | $\sigma(\%)$ |
|---|---|---|
| Tahifet | 1.16 | 19 |
| Imehrou | 1.13 | 17 |
| Golden | 1.38 | 18 |
| Boulder | 1.39 | 18 |
| Palo alto | 1.23 | 20 |

Imehrou, May and June for Golden and Boulder, January and December for Palo Alto – and those where these irradiances are very regular – October for the two sites Tahifet and Imehrou, September for Golden and Boulder, June for Palo Alto. These informations are very useful to refine the sizing of photovoltaic systems. Indeed, the anomalies in the operating of the photovoltaic systems installed in these sites appear during these months. There is for example for Tahifet excess of energy in October and storage is requested in June and December much more than in other months.

### 5.2.1 Annually and Monthly Classification Analysis

The thresholds $D_I$ and $D_{II}$ have first been determined for the sites of Tahifet and Imehrou. For this purpose, the heuristic method and the statistical one has been used, Table 2.3 gathers the thresholds obtained with the two methods. We notice that the empirical and statistical thresholds are very close. Since the empirical approach is very expensive in time to build histograms and to carry out their meticulous examination, we chose the statistical thresholds to classify the days of the studied sites. The obtained thresholds for all sites are illustrated by Table 2.4.

Table 2.5 gives the distribution of the probability of occurrence of daily solar irradiances for each class obtained from our classification. For Tahifet and Imehrou daily irradiances of class I have the largest probability of occurrence as compared to irradiances of the two other classes. These results confirm the pre-eminence of days with clear sky for the two sites; this is due to the climate of the south Algerian which is characterized by irradiances rarely fluctuated. However Class III (completely covered sky) is preponderant for the Californian sites. Class I is also important, whereas class II has less frequency of occurrence. These results demonstrate that the two

**Table 2.3** Fractal dimension thresholds obtained with the two methods: heuristic and statistic for Tahifet and Imehrou sites

| Site | $D_I$ (heuristic) | $D_I$ (statistic) | $D_{II}$ (heuristic) | $D_{II}$ (statistic) |
|---|---|---|---|---|
| Tahifet | 1.14 | 1.10 | 1.34 | 1.25 |
| Imehrou | 1.12 | 1.10 | 1.27 | 1.25 |

**Table 2.4** Statistical Fractal dimension thresholds for all studied sites

| Site | $D_I$ | $D_{II}$ |
|---|---|---|
| Tahifet | 1.14 | 1.34 |
| Imehrou | 1.12 | 1.27 |
| Golden | 1.35 | 1.49 |
| Boulder | 1.35 | 1.50 |
| Palo Alto | 1.19 | 1.37 |

**Table 2.5** Probability of occurrence of daily solar irradiance shapes of each class

| Site | Class I (%) | Class II (%) | Class III(%) |
|---|---|---|---|
| Tahifet | 58 | 16 | 26 |
| Imehrou | 62 | 16 | 21 |
| Golden | 24 | 22 | 53 |
| Boulder | 26 | 22 | 52 |
| Palo Alto | 49 | 17 | 34 |

studied sites are characterized by disturbed climate since the overcast sky days are preponderant at the two sites. At Palo Alto, classes I and III are pre-eminent which demonstrate that this site has a climate fairly disturbed.

On the accompanying CD, Tables of day's class are included for each studied site.

To validate the classification results, the average of the fractal dimension $<D>$, of clearness index $<K_T>$ and their standard deviations $\sigma(D)$ and $\sigma(K_T)$ have been computed for each class. They are summarized by Table 2.6.

These statistical properties show that our classification method leads to homogeneous groupings of the studied days since the standard deviations of $D$ and $K_T$ are weak compared to their averages. Indeed, in all the sites $\sigma(K_T)$ is lower than 10% for all classes and except for Golden and Boulder we note the same thing for $\sigma(D)$ but only for classes I and II. The more important value of this standard deviation for class III (upper than 10%) is due to the fact that this class contains rainy days whose irradiance signals have a regular form thus a fractal dimension near to 1 like already explained. For example, the shape of solar daily irradiance of class III

**Table 2.6** Mean value and standard deviation of $D$ and $K_T$ for the different classes of days

| | Site | Golden | | | Boulder | | | Tahifet | | | Imehrou | | | Palo Alto | | |
|---|---|---|---|---|---|---|---|---|---|---|---|---|---|---|---|---|
| | Class | I | II | III | I | II | III | I | II | III | I | II | III | I | II | III |
| Average | $<D>$ | 1.15 | 1.43 | 1.47 | 1.17 | 1.43 | 1.48 | 1.03 | 1.24 | 1.42 | 1.02 | 1.19 | 1.40 | 1.06 | 1.27 | 1.46 |
| | $<K_T>$ | 0.70 | 0.63 | 0.46 | 0.69 | 0.64 | 0.47 | 0.66 | 0.60 | 0.45 | 0.69 | 0.62 | 0.50 | 0.70 | 0.61 | 0.33 |
| Standard deviation | $\sigma(D)$ | 0.12 | 0.03 | 0.14 | 0.12 | 0.04 | 0.13 | 0.04 | 0.05 | 0.13 | 0.03 | 0.04 | 0.14 | 0.06 | 0.05 | 0.15 |
| | $\sigma(K_T)$ | 0.07 | 0.07 | 0.18 | 0.08 | 0.08 | 0.12 | 0.04 | 0.04 | 0.12 | 0.04 | 0.04 | 0.13 | 0.07 | 0.05 | 0.17 |

(see Fig. 2.8) corresponds to a rainy day in Golden. Its fractal dimension is equal to 1.11 and its related $K_T$ is 0.47. Using $D$, this daily irradiance should be classified in class II. But, when using $D$ and $K_T$ together it is categorized as class III. The fairly high values of $\sigma(D)$ for the class I in the two sites of Colorado is explained by the high value of $D_I$ due to the irradiances character of these sites which is very fluctuating.

In order to better characterize the three classes obtained our statistical analysis was refined by carrying out it on a monthly scale. In Table 2.7 monthly results of the frequency of each class, averages and standard deviations of the two parameters: $D$ and $K_T$ are presented. Table 2.7 shows that the distribution of the classes differs from a site to another.

As it can be observed from Table 2.7, Class III days have high frequency of occurrence for the sites Golden and Boulder, reaching a maximum in May and June. Only for the month September for Golden and February for Boulder class I have higher frequency of occurrences which are 51.6% and 39.3%, respectively. However, in Tahifet and Imehrou class I has higher frequency of occurrences for all the months, reaching maximum values in October and minimum in May and June.

In Palo Alto on the other hand we notice a seasonal distribution of the days. Indeed, class I presents high values in winter (January, February, November and December) where the maximum is detected in December and class III high values in summer (June–September).

These results are confirmed by the transition probabilities between two consecutive days having the same or different classes. For the two sites of Algeria, while transition probabilities from class I to the same class were quite high (65% and 40%), all other transitions were low. However for Golden and Boulder all transition probabilities are quite close in the ranges of 5 to 20%.

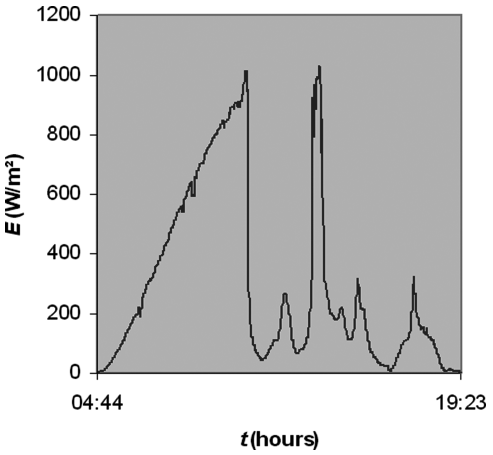


**Fig. 2.8** An example of a rainy day with an enough regular shape, $D = 1.11$ and $K_T = 0.47$

**Table 2.7** Monthly characteristics of each class obtained for the various sites

| | Site | Golden | | | Boulder | | | Tahifet | | | Imehrou | | | Palo Alto | | |
|---|---|---|---|---|---|---|---|---|---|---|---|---|---|---|---|---|
| | Class | I | II | III | I | II | III | I | II | III | I | II | III | I | II | III |
| January | Freq (%) | 19.4 | 25.8 | 54.8 | 19.4 | 22.6 | 58.0 | 64.5 | 12.9 | 22.6 | 58.1 | 12.9 | 29.0 | 12.9 | 22.6 | 64.5 |
| | $<D>$ | 1.20 | 1.44 | 1.39 | 1.16 | 1.45 | 1.43 | 1.02 | 1.25 | 1.47 | 1.02 | 1.17 | 1.42 | 1.18 | 1.25 | 1.49 |
| | $\sigma(D)$ | 0.15 | 0.03 | 0.16 | 0.10 | 0.05 | 0.14 | 0.23 | 0.06 | 0.10 | 0.03 | 0.02 | 0.12 | 0.01 | 0.05 | 0.14 |
| | $<K_T>$ | 0.60 | 0.58 | 0.36 | 0.65 | 0.62 | 0.40 | 0.69 | 0.60 | 0.34 | 0.66 | 0.60 | 0.39 | 0.59 | 0.59 | 0.28 |
| | $\sigma(K_T)$ | 0.05 | 0.05 | 0.14 | 0.07 | 0.04 | 0.16 | 0.15 | 0.05 | 0.15 | 0.03 | 0.05 | 0.15 | 0.06 | 0.03 | 0.13 |
| February | Freq (%) | 21.4 | 14.3 | 64.3 | 39.3 | 25.0 | 35.7 | 48.3 | 17.2 | 34.5 | 44.8 | 34.5 | 24.1 | 25.9 | 25.9 | 48.1 |
| | $<D>$ | 1.13 | 1.43 | 1.37 | 1.21 | 1.43 | 1.37 | 1.03 | 1.26 | 1.40 | 1.04 | 1.17 | 1.41 | 1.16 | 1.27 | 1.35 |
| | $\sigma(D)$ | 0.16 | 0.04 | 0.13 | 0.13 | 0.04 | 0.16 | 0.23 | 0.05 | 0.07 | 0.04 | 0.03 | 0.19 | 0.01 | 0.05 | 0.10 |
| | $<K_T>$ | 0.66 | 0.65 | 0.41 | 0.68 | 0.66 | 0.42 | 0.69 | 0.62 | 0.49 | 0.66 | 0.64 | 0.52 | 0.63 | 0.60 | 0.25 |
| | $\sigma(K_T)$ | 0.07 | 0.06 | 0.14 | 0.12 | 0.11 | 0.18 | 0.15 | 0.02 | 0.13 | 0.03 | 0.05 | 0.09 | 0.03 | 0.05 | 0.14 |
| March | Freq (%) | 12.9 | 35.5 | 51.6 | 19.4 | 29.0 | 51.6 | 54.8 | 12.9 | 32.3 | 45.2 | 12.9 | 41.9 | 45.2 | 32.3 | 22.6 |
| | $<D>$ | 1.13 | 1.43 | 1.48 | 1.19 | 1.42 | 1.45 | 1.01 | 1.24 | 1.43 | 1.04 | 1.19 | 1.39 | 1.07 | 1.29 | 1.47 |
| | $\sigma(D)$ | 0.10 | 0.03 | 0.16 | 0.11 | 0.04 | 0.19 | 0.01 | 0.07 | 0.18 | 0.04 | 0.06 | 0.15 | 0.05 | 0.06 | 0.15 |
| | $<K_T>$ | 0.69 | 0.66 | 0.43 | 0.72 | 0.70 | 0.50 | 0.65 | 0.61 | 0.39 | 0.67 | 0.57 | 0.41 | 0.68 | 0.62 | 0.38 |
| | $\sigma(K_T)$ | 0.02 | 0.04 | 0.23 | 0.09 | 0.08 | 0.21 | 0.04 | 0.03 | 0.11 | 0.04 | 0.04 | 0.12 | 0.04 | 0.04 | 0.12 |
| April | Freq (%) | 13.3 | 30.0 | 56.7 | 16.7 | 30.0 | 53.3 | 60.0 | 16.7 | 23.3 | 76.7 | 0.00 | 23.3 | 20.0 | 13.3 | 66.7 |
| | $<D>$ | 1.19 | 1.42 | 1.48 | 1.17 | 1.41 | 1.49 | 1.03 | 1.19 | 1.46 | 1.02 | | 1.44 | 1.08 | 1.28 | 1.48 |
| | $\sigma(D)$ | 0.18 | 0.02 | 0.10 | 0.15 | 0.04 | 0.11 | 0.04 | 0.04 | 0.08 | 0.03 | | 0.11 | 0.06 | 0.02 | 0.14 |
| | $<K_T>$ | 0.76 | 0.64 | 0.49 | 0.74 | 0.66 | 0.51 | 0.67 | 0.63 | 0.51 | 0.70 | | 0.53 | 0.68 | 0.65 | 0.46 |
| | $\sigma(K_T)$ | 0.07 | 0.08 | 0.19 | 0.10 | 0.09 | 0.18 | 0.03 | 0.01 | 0.10 | 0.04 | | 0.17 | 0.07 | 0.09 | 0.13 |

**Table 2.7** (continued)

| | Site | Golden | | | Boulder | | | Tahifet | | | Imehrou | | | Palo Alto | | |
|---|---|---|---|---|---|---|---|---|---|---|---|---|---|---|---|---|
| | Class | I | II | III | I | II | III | I | II | III | I | II | III | I | II | III |
| May | Freq (%) | 3.23 | 19.3 | 77.4 | 6.50 | 12.9 | 80.6 | 41.9 | 38.7 | 19.4 | 51.6 | 29.0 | 19.4 | 54.8 | 16.1 | 29.0 |
| | $<D>$ | 1.34 | 1.43 | 1.50 | 1.29 | 1.42 | 1.54 | 1.04 | 1.21 | 1.39 | 1.02 | 1.17 | 1.32 | 1.03 | 1.30 | 1.52 |
| | $\sigma(D)$ | 0.00 | 0.04 | 0.13 | 0.07 | 0.06 | 0.09 | 0.04 | 0.05 | 0.15 | 0.02 | 0.04 | 0.14 | 0.04 | 0.02 | 0.10 |
| | $<K_T>$ | 0.73 | 0.66 | 0.49 | 0.68 | 0.67 | 0.50 | 0.65 | 0.60 | 0.53 | 0.68 | 0.64 | 0.60 | 0.76 | 0.65 | 0.52 |
| | $\sigma(K_T)$ | 0.00 | 0.10 | 0.17 | 0.03 | 0.08 | 0.17 | 0.03 | 0.04 | 0.07 | 0.05 | 0.04 | 0.09 | 0.06 | 0.10 | 0.15 |
| June | Freq (%) | 16.7 | 13.3 | 70.0 | 13.3 | 23.3 | 63.3 | 36.7 | 26.7 | 36.7 | 36.7 | 40.0 | 23.3 | 96.7 | 3.30 | 0.00 |
| | $<D>$ | 1.22 | 1.46 | 1.48 | 1.21 | 1.44 | 1.53 | 1.05 | 1.25 | 1.42 | 1.04 | 1.21 | 1.46 | 1.04 | 1.21 | |
| | $\sigma(D)$ | 0.11 | 0.02 | 0.14 | 0.09 | 0.04 | 0.10 | 0.04 | 0.04 | 0.09 | 0.04 | 0.05 | 0.13 | 0.04 | 0.00 | |
| | $<K_T>$ | 0.60 | 0.59 | 0.49 | 0.65 | 0.61 | 0.47 | 0.59 | 0.57 | 0.52 | 0.68 | 0.63 | 0.57 | 0.77 | 0.56 | |
| | $\sigma(K_T)$ | 0.08 | 0.06 | 0.20 | 0.10 | 0.09 | 0.16 | 0.03 | 0.05 | 0.07 | 0.02 | 0.04 | 0.06 | 0.03 | 0.00 | |
| July | Freq.(%) | 35.5 | 22.6 | 41.9 | 25.8 | 22.6 | 51.6 | 48.4 | 3.20 | 48.4 | 71.0 | 9.70 | 19.4 | 80.6 | 9.70 | 9.70 |
| | $<D>$ | 1.16 | 1.41 | 1.43 | 1.14 | 1.44 | 1.44 | 1.04 | 1.19 | 1.33 | 1.03 | 1.19 | 1.34 | 1.02 | 1.28 | 1.42 |
| | $\sigma(D)$ | 0.12 | 0.04 | 0.16 | 0.13 | 0.06 | 0.11 | 0.05 | 0.00 | 0.11 | 0.04 | 0.05 | 0.19 | 0.03 | 0.07 | 0.04 |
| | $<K_T>$ | 0.69 | 0.61 | 0.54 | 0.67 | 0.62 | 0.51 | 0.60 | 0.52 | 0.42 | 0.69 | 0.64 | 0.48 | 0.77 | 0.66 | 0.49 |
| | $\sigma(K_T)$ | 0.08 | 0.07 | 0.12 | 0.09 | 0.07 | 0.11 | 0.03 | 0.00 | 0.09 | 0.03 | 0.02 | 0.14 | 0.03 | 0.07 | 0.19 |
| August | Freq.(%) | 22.6 | 29.0 | 48.4 | 29.0 | 22.6 | 48.4 | 58.1 | 29.0 | 12.9 | 83.9 | 12.9 | 3.20 | 80.6 | 12.9 | 6.50 |
| | $<D>$ | 1.13 | 1.45 | 1.49 | 1.23 | 1.43 | 1.48 | 1.02 | 1.25 | 1.40 | 1.02 | 1.21 | 1.30 | 1.02 | 1.26 | 1.49 |
| | $\sigma(D)$ | 0.12 | 0.03 | 0.10 | 0.11 | 0.03 | 0.11 | 0.04 | 0.06 | 0.13 | 0.04 | 0.02 | 0.00 | 0.03 | 0.08 | 0.07 |
| | $<K_T>$ | 0.70 | 0.61 | 0.49 | 0.68 | 0.61 | 0.48 | 0.67 | 0.59 | 0.47 | 0.71 | 0.64 | 0.68 | 0.72 | 0.65 | 0.55 |
| | $\sigma(K_T)$ | 0.07 | 0.08 | 0.11 | 0.08 | 0.06 | 0.11 | 0.02 | 0.05 | 0.09 | 0.02 | 0.03 | 0.00 | 0.03 | 0.08 | 0.04 |

**Table 2.7** (continued)

| | Site | Golden | | | Boulder | | | Tahifet | | | Imehrou | | | Palo Alto | | |
|---|---|---|---|---|---|---|---|---|---|---|---|---|---|---|---|---|
| | Class | I | II | III | I | II | III | I | II | III | I | II | III | I | II | III |
| September | Freq.(%) | 50.0 | 16.7 | 33.3 | 46.7 | 16.7 | 36.7 | 66.7 | 10.0 | 23.3 | 60.0 | 20.0 | 20.0 | 90.0 | 0.00 | 10.0 |
| | $<D>$ | 1.09 | 1.43 | 1.48 | 1.10 | 1.46 | 1.49 | 1.04 | 1.27 | 1.41 | 1.03 | 1.23 | 1.36 | 1.04 | | 1.30 |
| | $\sigma(D)$ | 0.09 | 0.04 | 0.17 | 0.11 | 0.06 | 0.12 | 0.05 | 0.05 | 0.09 | 0.03 | 0.03 | 0.08 | 0.04 | | 0.25 |
| | $<K_T>$ | 0.74 | 0.68 | 0.20 | 0.74 | 0.65 | 0.47 | 0.67 | 0.57 | 0.55 | 0.70 | 0.63 | 0.58 | 0.65 | | 0.45 |
| | $\sigma(K_T)$ | 0.02 | 0.07 | | 0.03 | 0.07 | 0.14 | 0.04 | 0.05 | 0.11 | 0.01 | 0.03 | 0.09 | 0.05 | | 0.19 |
| October | Freq.(%) | 51.6 | 9.70 | 38.7 | 38.7 | 16.1 | 45.2 | 100 | 0.00 | 0.00 | 87.1 | 3.20 | 9.70 | 67.7 | 19.4 | 12.9 |
| | $<D>$ | 1.15 | 1.41 | 1.50 | 1.14 | 1.42 | 1.50 | 1.01 | | | 1.01 | 1.16 | 1.43 | 1.12 | 1.29 | 1.46 |
| | $\sigma(D)$ | 0.13 | 0.04 | 0.13 | 0.11 | 0.06 | 0.11 | 0.03 | | | 0.02 | 0.00 | 0.13 | 0.05 | 0.03 | 0.06 |
| | $<K_T>$ | 0.73 | 0.64 | 0.47 | 0.71 | 0.68 | 0.48 | 0.68 | | | 0.71 | 0.63 | 0.61 | 0.63 | 0.58 | 0.46 |
| | $\sigma(K_T)$ | 0.04 | 0.07 | 0.21 | 0.05 | 0.03 | 0.20 | 0.02 | | | 0.02 | 0.00 | 0.07 | 0.02 | 0.02 | 0.14 |
| November | Freq.(%) | 20.0 | 20.0 | 60.0 | 23.3 | 20.0 | 56.7 | 63.3 | 16.7 | 20.0 | 80.0 | 3.30 | 16.7 | 0.00 | 40.0 | 60.0 |
| | $<D>$ | 1.13 | 1.44 | 1.53 | 1.16 | 1.45 | 1.50 | 1.02 | 1.24 | 1.47 | 1.01 | 1.13 | 1.42 | | 1.26 | 1.46 |
| | $\sigma(D)$ | 0.14 | 0.04 | 0.11 | 0.12 | 0.05 | 0.13 | 0.03 | 0.03 | 0.09 | 0.02 | 0.00 | 0.10 | | 0.03 | 0.16 |
| | $<K_T>$ | 0.70 | 0.63 | 0.46 | 0.68 | 0.65 | 0.41 | 0.68 | 0.61 | 0.42 | 0.69 | 0.63 | 0.48 | | 0.59 | 0.28 |
| | $\sigma(K_T)$ | 0.07 | 0.08 | 0.22 | 0.07 | 0.08 | 0.18 | 0.02 | 0.04 | 0.13 | 0.02 | 0.00 | 0.11 | | 0.02 | 0.14 |
| December | Freq.(%) | 25.8 | 29.0 | 45.2 | 32.3 | 22.6 | 45.2 | 51.6 | 6.50 | 41.9 | 54.8 | 19.4 | 25.8 | 9.70 | 12.9 | 77.4 |
| | $<D>$ | 1.16 | 1.42 | 1.50 | 1.16 | 1.43 | 1.48 | 1.04 | 1.28 | 1.49 | 1.03 | 1.19 | 1.44 | 1.13 | 1.28 | 1.46 |
| | $\sigma(D)$ | 0.12 | 0.03 | 1.50 | 0.11 | 0.04 | 0.14 | 0.05 | 0.11 | 0.17 | 0.03 | 0.06 | 0.12 | 0.04 | 0.06 | 0.17 |
| | $<K_T>$ | 0.68 | 0.62 | 0.46 | 0.67 | 0.61 | 0.45 | 0.66 | 0.42 | 0.42 | 0.65 | 0.59 | 0.51 | 0.58 | 0.58 | 0.21 |
| | $\sigma(K_T)$ | 0.08 | 0.05 | 0.46 | 0.06 | 0.05 | 0.17 | 0.02 | 0.09 | 0.10 | 0.04 | 0.04 | 0.09 | 0.06 | 0.02 | 0.12 |

## 6 Conclusions

In this chapter, a classification procedure for solar irradiances is presented and discussed for five locations. This procedure uses fractal dimension analysis. A new method of estimating fractal dimensions is utilized which gives satisfactory results. This method based on covering multi scale, using rectangles as the structuring element. The method is tested for two well-known functions and an average error of 3.7% is obtained for over 180 tests.

The validation of the classification method is carried out by annual and monthly analysis using the fractal dimension and the clearness index of the daily irradiances. Three different classes of the days are determined to be a reasonable classification. Results for the sites with similar climates give the same type of classifications of the days as it is observed from their annual and monthly average classification parameters. Observed standard deviations of the monthly parameters from an annual mean value are relatively small.

Classification of the daily solar irradiance is important in design and installation of solar energy systems, especially PV arrays. Trends in the patterns of daily solar irradiance became significant information due to the recent interests in renewable technologies. This interest is essentially due to global warming and other negative effects to our environment. Such analyses presented in this chapter are of great interest as they reduce the initial costs by appropriate design and construction of solar energy systems suitable to the climate of the site of interest.

## References

Aguiar RJ, Collores-Pereira M, Conde JP (1988) Simple procedure for generating sequences of daily radiation values using a library of Markov transition Matrices. Solar Energy 40:269–279

Bartoli B, Coluzzi B, Cuomo V, Francesca M, Serio S (1981) Autocorrelation of daily global solar radiation. II Nuovo Cimento, 4C:113–122

Berry MV, Lewis ZV (1980). On the Weierstrass–Mandelbrot fractal function. Proc roy Soc Ser a 370:459–484

Bouligand G (1928) Ensembles impropres et nombre dimensionnel. Bull Sci Math II-52: 320–344, 361–376

Bouroubi MY (1998) Modélisation de l'irradiation solaire à l'échelle journalière et horaire, pour l'Algérie. Master thesis, USTHB University

Brinkworth BJ (1977) Autocorrelation and stochastic modelling of insolation sequences. Solar Energy 19:343–347

CPAU, 2007, http://www.cpau.com/programs/pv-partners/pvdata.html

Dubuc B, Quiniou F, Roques-Carmes C, Tricot C, Zucker SW (1989) Evaluating the fractal dimension of profiles. Phys Rev A 39:1500–1512

Guessoum AS, Boubekeur A, Maafi A (1998) Global irradiation model using radial basis function neural networks. In Proceedings of World Renewable Energy Congress V (WREC'98), Florence (Italy), pp 169–178

Hardy GH (1916) Weierstrass's nondifferentiable function. Trans amer Math Soc 17:322–323

Harrouni S, Guessoum A (2003) Fractal Classification of solar irradiances into typical days using a cumulative distribution function. ICREPQ'03, Vigo (Spain)

Harrouni S, Guessoum A (2006) New method for estimating the time series fractal dimension: Application to solar irradiances signals. In: Solar Energy: New research Book. Nova Science Publishers, New York, pp 277–307

Harrouni S, Guessoum A, Maafi A (2002) Optimisation de la mesure de la dimension fractale des signaux: Application aux éclairements solaires. SNAS'02, Université d'Annaba

Harrouni S, Guessoum A, Maafi A (2005) Classification of daily solar irradiation by fractional analysis of 10–min–means of solar irradiance. Theoretical and Applied Climatology 80: 27–36

Harrouni S, Maafi A (2002) Classification des éclairements solaires à l'aide de l'analyse fractale. Revue Internationale des énergies renouvelables (CDER) 5:107–122

Huang Q, Lorch JR, Dubes RC (1994) Can the fractal dimension of images be measured?. Pattern Recognition 27:339–349

Kolhe M, Agbossou K, Hamelin J, Bose TK (2003) Analytical model for predicting the performance of photovoltaic array coupled with a wind turbine in a stand-alone renewable energy system based on hydrogen. Renewable Energy 28:727–742

Lestienne R, Bois Ph, Obled Ch (1979) Analyse temporelle et cartographie de la matrice stochastique pour le modèle Markovien dans le midi de la France. La Météorologie 17:83–122

Liebovitch LS, Toth A (1989) Fast algorithm to determine fractal dimension by box counting. Phys Lett A 14:386–390

Liu BYH, Jordan RC (1963) The long-term average performance of flat-plate solar-energy collectors: With design data for the US its outlying possessions and Canada. Solar Energy 7:53–74

Louche A, Notton G, Poggi P, Simonot G (1991) Classification of direct irradiation days in view of energetic applications. Solar Energy 46:255–259

Lundahl T, Ohley WJ, Kay SM, Siffert R (1986) Fractional Brownian motion: A maximum likelihood estimator and its application to image texture. IEEE Trans Med Imaging MI-5:152–160

Maafi A (1991) Mise en évidence d'aspects physiques du modèle Markovien du premier ordre à deux états en météorologie solaire: Application à la conversion photovoltaïque. Doctorat thesis, USTHB University

Maafi A (1998) Markov-Models in discrete time for solar radiation. In Proceedings of Multiconference on Computational Engineering in Systems Applications (IMACS–IEEE), Nabeul-Hammamet (Tunisia) pp 319–322

Maafi A, Harrouni S (2000) Measuring the fractal dimension of solar irradiance in view of PV systems performance analysis. Proc 6th W REC, Brighton (UK), pp 2032–2035

Maafi A, Harrouni S (2003) Preliminary results of fractal classification of daily solar irradiance. Solar Energy 75:53–61

Mandelbrot B (1967) How Long Is the Coast of Britain? Statistical Self-Similarity and Fractional Dimension. Science, New Series 156:636–638

Mandelbrot BB (1982/1983) The fractal geometry of nature, Freeman, New York

Mandelbrot BB, Wallis JR (1969) Computer experiments with fractional Brownian motion. Water Resources Res 5:228–267

Maragos P, Sun FK (1993) Measuring the fractal dimension of signals: morphological covers and iterative optimization. IEEE Transaction on Signal Processing 41:108–121

MIDC, 2007, http://www.nrel.gov/midc/

Minkowski H (1901) Uber die Bgriffe Lange, Oberflache und Volumen, Jahresber, Deutch. Mathematikerverein 9:115–121

Muselli M, Poggi P, Notton G, Louche A (2000) Classification of typical meteorological days from global irradiation records and comparison between two Mediterranean coastal sites in Corsica Island. Energy Conversion and Management 41:1043–1063

Richardson LF (1961) The problem of contiguity: an appendix of statistics of deadly quarrels. Genmal Systems Yearbook 6:139–187

Sayigh AAM (1977) Solar energy engineering chap 4. Academic Press, New York

Sfetsos A, Coonick AH (2000) Univariate and multivariate forecasting of hourly solar radiation with artificial intelligence techniques. Solar Energy 68:169–178

Tricot C, Quiniou JF, Wehbi D, Roques-Carmes C, Dubuc B (1988) Evaluation de la dimension fractale d'un graphe. Rev Phys 23:111–124

Voss RF (1988) Fractals in nature: From characterization to simulation. In The science of fractal Images, HO Peitgen and D Saupe. Springer-Verlag, New York

Zeng X, Koehl L, Vasseur C (2001) Design and implementation of an estimator of fractal dimension using fuzzy techniques. Pattern Recognition 34:151–169

http://www.springer.com/978-3-540-77454-9

Modeling Solar Radiation at the Earth's Surface
Recent Advances
Badescu, V. (Ed.)
2008, XXXIII, 517 p. With online files/update., Hardcover
ISBN: 978-3-540-77454-9